Block copolymer ordering on elastomeric substrates of tunable surface energy

Arzu Hayirlioglu [1,2] · Manish Kulkarni [3] · Gurpreet Singh [1,4] · Abdullah M. Al-Enizi [5] · Irina Zvonkina [6] · Alamgir Karim [6]

Abstract

We report a range of surface characteristics from strong and partial dewetting to complete wetting for thin films of cylinder and lamellae forming block copolymers (c-BCP and l-BCP, respectively) of polystyrene-*b*-polymethylmethacrylate (PS-*b*-PMMA) on flexible substrates. BCP of various molecular weights (Mw) was applied on elastomeric polydimethylsiloxane (PDMS) substrates of distinct cross-link densities and various surface energy (SE) obtained by exposure to UV-ozone. We demonstrate that lower Mw c-BCP films dewet faster than l-BCP films of higher Mw applied on PDMS of lowest cross-link density and SE < 25 mJ/m^2. Partial dewetting was observed for c-BCP films applied on the lowest cross-link density substrates with 25 mJ/m^2 < SE < 32 mJ/m^2, with a sharper transition from dewetting to wetting for l-BCP films. Finally, complete wetting (stable films) occurred for both c-BCP and l-BCP films on PDMS substrates with lowest cross-link density and SE > 32 mJ/m^2, as well as on PDMS of the highest cross-link density with SE > 25 mJ/m^2. In this extended SE wetting regime, c-BCP show vertical orientation when applied on both types of cross-linked PDMS in a narrow neutral SE range (39–40) mJ/m^2, while being oriented parallel to the substrate when SE > 40 mJ/m^2. The ratio of vertically oriented l-BCP however decreases gradually when applied on substrates with a higher SE range (40–65 mJ/m^2) in comparison to the sharply transitioning c-BCP orientation, reflecting the intrinsic stability of vertical lamellae over a wider range of substrate SE, consistent with theoretical estimates. These results have important ramifications for design of next-generation flexible electronics utilizing BCP thin films.

Keywords Block copolymer · Surface energy · PDMS film · BCP ordering · Polymer thin films

1 Introduction

Block copolymer films have a unique capability of self-assembly which makes them facile soft materials and a topic of current interest. They can effectively be remolded into well-defined, ordered nanostructures, such as cylindrical, spherical, or lamellar, in which the microstructure and the domain size can be controlled by the composition and strength of interactions of the blocks [1–3]. This adjustable morphology makes BCPs sought after in a variety of applications with advantageous characteristics that can compete with devices produced by current lithography technologies [4]. Ordering BCP films is envisioned to be particularly advantageous in fields using high-end technology, e.g., in the energy storage and conversion field, one envisions advanced fuel cells [5], photovoltaic devices [6], capacitors [7], high-density data storage devices [4], etc. Various methods of inducing ordering in BCP are currently used, ranging from chemical patterning [8, 9], electrical and magnetic fields [10, 11] to lithography [12, 13], depending on the particular application.

BCP ordering and orientation in thin films have been intensively studied on supporting hard substrates such as glass, silicon, quartz, etc. [14–16]. Flexible electronics has harnessed much interest with research focus based on nanotechnology, harmonious with flexible materials and substrates. Related to it, the shortcomings of most traditionally used

✉ Alamgir Karim
akarim3@central.uh.edu

1 Department of Polymer Engineering, University of Akron, Akron, OH 44325, USA

2 Present address: Avery Dennison Corporation, Mentor, OH 44060, USA

3 Indian Institute of Technology, Kanpur, Kanpur, UP 208016, India

4 Present address: Intel Corporation, Hillsboro, OR 97124, USA

5 Chemistry Department, Faculty of Science, King Saud University, 2455, Riyadh 11451, Saudi Arabia

6 Department of Chemical and Biomolecular Engineering, University of Houston, Houston, TX 77203, USA

substrate materials are brittleness and stiffness that have limitations for flexible display technologies. Research on thin BCP films applied on substrates having bendable features, as well as more recently used elastomeric substrates exhibiting compressible, stretchable, and deformable properties is evolving. The most commonly used flexible materials as substrates in industries are PET, Kapton® (DuPont™), and PDMS. Among them, PET is known for excellent barrier, tensile strength, and thermal stability properties, whereas Kapton has good mechanical strength. However, PDMS has definite select benefits over the other two substrates, like non-toxicity, chemically inert nature, transparency, biocompatibility, lightweight, low cost, and flexible attributes. Hence, they have been used in a wide range of applications such as membranes [17], biomedical devices [18–21], and electronics industry [22–25]. PDMS exhibits excellent conformal contact characteristics as well by virtue of its flexibility. Additionally, its modulus as well as flexibility and surface energy, in comparison to PET and Kapton, can be modified according to the specific requirements. For instance, by changing the ratio of the oligomer to the cross-linking agent for PDMS thermal curable compositions, the modulus of PDMS can be altered in the range of 1–10 Mpa.

One of the approaches to fabrication of flexible electronics devices was demonstrated by Rogers et al. via placement of buckled ultrathin layers made by brittle silicon nanowires, nanoribbons, or membranes on elastomeric PDMS substrates that have the ability to stretch and compress [26, 27]. Russell et al. showed another route to creating long-range ordered structures on flexible polymeric materials by ordering BCP films on sawtooth patterned polymeric replicas [28]. Recently, Singh et al. developed alternative methods to orient vertical PS-*b*-PMMA BCP films on hard (Si, quartz) and flexible (Kapton, PDMS) substrates via sharp dynamic cold zone annealing with sharp thermal gradient (CZA-S) [14], as well as PS-P2VP films on PDMS and Kapton via CZA in soft shear mode (CZA-SS) [29]. In that research, BCP thin film stability and orientation on flexible substrates were systematically examined for flexible polymeric (PDMS) substrates of different chemical compositions and mechanical properties, under dynamic thermal annealing conditions.

In contrast to bulk systems, stable BCP films are not only affected by the film thickness and domain spacing, but also by interfacial interactions [30]. Modification of the substrate surface energy enables for control of orientation of the BCP and thin films morphology and properties. The stability of thin polymeric films towards dewetting, prepared with either homopolymer or block copolymer, is closely related to the film wettability property on the substrate. Wetting or dewetting from the substrate can happen as a consequence of interaction with the polymer film based on the interfacial interaction amidst the substrate and the film as a function of the film thickness.

Dewetting of liquid or solid films usually occurs via formation of free substrate surface regions within the film, as the film becomes unstable, that can be explained in terms of decreasing the Gibbs free energy of the system. In the second order derivative of the Gibbs free energy (ΔG) w.r.t. the film thickness h, if negative, the film turns out to be unstable: $d^2 \Delta G / dh^2 < 0$. Otherwise, the film can be thermodynamically metastable or stable [31, 32]. In general, the interactions between a thin film and a hard substrate can be explained by the spreading parameter, S, which is calculated by the following equation, $S = \gamma_B - (\gamma_A + \gamma_{AB})$ where γ_A and γ_B indicate the surface tension of the film (A) and the substrate (B), respectively. The interfacial tension at the polymer/substrate interface is given by γ_{AB}. When the spreading parameter, S, becomes greater than zero (S > 0), the polymer film starts wetting the substrate and becomes stable. If the spreading parameter is smaller than zero (S < 0), it implies that the polymer film is unstable and will dewet from the substrate with formation of holes and ultimately droplets [33]. A typical polymer dewetting can involve either of two types of mechanisms, such as hole formation via nucleation and spinodal dewetting due to fluctuations in ultrathin film [31, 34, 35]. Green et al. showed the dewetting of a disordered block copolymer thin film occurred at different stages by an autophobic mechanism with formation of a dense brush layer. Dewetting of PS-*b*-PMMA diblock copolymer films was studied as a function of the film thickness and interactions at substrate and air interfaces on hard silicon and on chemically modified substrates [31, 36–38].

Several researchers have shown the substrate modification methods for BCP affects their ordering, orientation, and long-range order, which is important for several applications, like in electronics. Usually, observation of the perpendicular orientation of BCP system on the substrate is noted for the case when the substrate surface is neutral with respect to the blocks. If one of the blocks preferentially wets the substrate or air surface, parallel orientation is observed within the film at that interface. In these systems, the properties of the substrates can be organized in terms of both chemical or physical nature, individually or by their combinations, to acquire the desired orientation. Microstructures can be ordered and aligned for block copolymers in particular directions as they are highly reliant on the interfacial energies arising from the surface boundaries. Several chemical methods, such as neutral brushes, self-assembly monolayers, and chemical patterning can be used to obtain this efficiently.

Mansky et al. and other researchers have performed extensive theoretical and practical studies on random copolymer brush layer grafted onto the substrate and film interfaces to control the interactions between them [39–41]. These systems have the potential to affect a gradual substrate modification by creating a range of surface energy values. Russell and coworkers have exclusively considered this

phenomenon with the purpose of creating perpendicular orientation of PS-*b*-PMMA BCP by forming a neutral layer on the substrate with grafted PS-*r*-PMMA on the silicon surface [42–45]. This idea was to further develop such double neutral surfaces comprising of random copolymer brushes to heighten the perpendicular orientation all along the BCP film [42]. The power of these interfacial interactions is usually altered by exchanging each block composition from the random brushes. It has been shown for the block copolymer films coated on PS-*r*-PMMA modified substrate rich in PS, symmetric wetting due to PS block interaction, and for those random brush films rich in PMMA an anti-symmetric wetting occurs due to favorable interactions of PMMA blocks with the substrate surface [43–45].

Chemical patterning is another method to change the substrate characteristics and to align BCP thin films. Kim et al. used self-assembly monolayers (SAMs) as one of the materials, coated on the substrate to create hydrophilic (OH-terminated) and hydrophobic (CH$_3$-terminated) stripes via micro-contact printing [46]. Heier et al. showed island formation in PS-*b*-P2VP films over the OH-terminated stripes [47]. On the other hand, Nealey and coworkers showed self-assembly of symmetric PS-*b*-PMMA films on patterned octadecyltrichlorosilane (OTS) coated substrates, where extreme ultraviolet interferometry lithography (EUV-IL) was used to pattern the OTS surface. Lamellar PS and PMMA blocks of a BCP film wet either CH$_3$- or OH-terminated regions because of the unexposed and exposed UV regions, leading to perpendicular orientation on the substrate [9]. Moreover, combinatorial gradient methods have been developed by Karim et al. to create a 2D map of the neutral vertical regime, and symmetric and asymmetric parallel lamellar regimes for PS-*b*-PMMA morphology, depending on the film thickness and on the substrate surface energy altered by using UV-ozone treatment [48].

In this work, we studied the cylindrical and lamellar forming BCP (c-BCP and l-BCP, respectively) thin films morphology and wetting properties on flexible PDMS substrates with controlled surface energy and controlled flexibility with select cross-link density. As there are only limited studies on morphology of BCP applied on polymeric substrates, there is a lack of knowledge on how the BCP film wetting behavior on flexible polymeric substrates is affected by the surface energy and cross-link density of the substrate, to determine the effects arising from the compositional and surface energy mismatch for the cylindrical and lamellar BCP systems on such substrates. Specifically, we explore the regimes of the PS-*b*-PMMA film dewetting, transition, and wetting by changing gradually the PDMS substrate surface energy from 20 to 70 mJ/m^2. For the wetting regime, we examine how to control the orientation of c-BCP and l-BCP by changing the PDMS substrate surface energy and its mechanical modulus through degree of cross-linking.

2 Experimental

2.1 Preparation of polydimethyl siloxane substrates

Sylgard 182 Silicone Elastomer kit was used to prepare PDMS substrates as advised by the manufacturer (Dow Corning) with the mass ratio of the base oligomer to the curing agent as 10:1 (~ 10 wt%) and 25:1 (~ 4 wt%). The oligomer and the curing agent were mixed and degassed for 30 min under vacuum. PDMS samples were prepared by both spin coating at 3000 rpm for 50 s and flow coating on glass substrates, and cured at 120 °C for 2 h. PDMS compositions consisting of 4 wt% of the cross-linking agent were coated directly on the glass substrate. On the other hand, PDMS compositions consisting of 10 wt% of the cross-linking agent were poured onto silanized glasses and the peeled-off smooth side of the elastomeric substrates was used for subsequent experiments.

2.2 Surface treatment of PDMS substrates

In order to alter the wetting properties of PDMS from hydrophobic to hydrophilic and to enhance adhesion between the BCP films and the PDMS substrates, the substrate surface needs to be treated. In our studies, we used a UV-ozone system (Novascon PSD Series) as the surface treatment method. The UVO treatment times were selected as 1, 2, 3, 4, 5, 6, and 8 h. It is important to note that using a high power UV source can reduce these exposure periods of time. The surface energy was calculated by performing contact angle measurements based on the static sessile drop method data with the drop volume of 3 μl after using goniometer (Rame-Hart Goniometer). Diionized water, hexadecane, dimehtylsulfoxide, and diiodomethane were used as liquids for the contact angle measurements to determine the surface energy.

2.3 Preparation of BCP thin films

Two BCP systems were used in this study: PS-*b*-PMMA BCP of MW (Mn) of 35-*b*-12.5 kg/mol (total 47.5 kg/mol) that typically forms cylinders (c-BCP) of polydispersity index of $M_w/M_n = 1.07$, and of MW (Mn) of 33-*b*-33 kg/mol (total 66 kg/mol) that forms lamellae (l-BCP) of polydispersity index of $M_w/M_n = 1.09$. Both BCP systems were obtained from Polymer Source, Inc. The cylinder to cylinder distance was $L_0 \approx 24$ nm for 47.5 kg/mol and the lamellar domain spacing was $L_0 \approx 35$ nm for 66 kg/mol. Samples of both types of BCP were dissolved in toluene (Laboratory grade) with a total polymer concentration of 2 wt% and stirred overnight. Afterwards, the polymer solutions were filtered using a 0.2 μm PTFE filter. BCP films which were uniformly thin were developed by spin coating of all the solutions at the same speed (1000 rpm), acceleration and time (50 s) on the previously prepared (see above) PDMS

substrates surface immediately after UVO treatment in order to avoid any surface alterations of the substrates. The cylindrical and lamellar PS-*b*-PMMA thin films had film thicknesses of 85 nm and 75 nm, respectively, verified by Filmetrics F-20 UV Thin Film Analyzer. In view of the glass transition temperature of the blocks (100 °C), the annealing temperatures were determined for the BCP systems. All the thin BCP films were annealed at 160 °C for 14 h under vacuum.

2.4 FTIR spectroscopy and microscopy image analysis

The FTIR spectroscopy was performed using a Thermo Electron Corporation spectrometer (Thermo Scientific Inc.), in the absorption mode, in order to characterize the surface chemical composition of the PDMS substrates exposed to UVO. The baseline correction was performed initially for the surface of the thermally cured PDMS slabs. The FTIR spectra of the samples exposed to UVO for different periods of time and for PDMS without the UVO treatment show the characteristic absorption peaks marked as (1)–(9) in Fig. 1. A strong peak (1) is connected with –CH_3 rocking (785–815 cm^{-1}). Peaks (2) and (3) are related with $\equiv$Si–OH stretching (825–870 cm^{-1} and 870–920 cm^{-1}, respectively). A strong doublet peak (4–5) related to asymmetric $\equiv$Si–O–Si$\equiv$ stretching (1015–1090 cm^{-1}), a weak transition occurring at band 6 is linked with –CH_2– vibration (1150–1200 cm^{-1}) and a single peak (7) corresponds to the symmetric –CH_3 stretching in $\equiv$Si–CH_3 (1245–1270 cm^{-1}). A distinct peak (8) is demonstrates an asymmetric –CH_3 stretching in $\equiv$Si–CH_3 (2950–2970 cm^{-1}).

The optical microscopy images of the BCP films were collected using an Olympus BX-41 microscope in the transmission mode under the bright field. The structure of the BCP

films on the PDMS substrates was characterized using a DI-Veeco Nanoscope V AFM at the Akron Functional Materials Center, and the Grazing-incidence small-angle X-ray scattering (GISAXS) measurements were performed at the X9 beamline of the National Synchrotron Light Source (NSLS) at the Brookhaven National Laboratory. An incident X-ray beam of 13.5 keV at the wavelength of 0.0918 nm was used, and the analysis of the samples was carried out under vacuum (~40 Pa). The GISAXS experiments were accomplished at 0.15° incidence angle, i.e., performed above the film-vacuum critical angle, to specifically observe the BCP ordering through the entire film thickness, using a charge-coupled device (CCD) detector for the data collection.

3 Results and discussion

In this study, two types of polydimethlysiloxane (PDMS) with distinct compositions and cross-link degree and, therefore, different modulus and flexibility [49], as well as surface characteristics, were used as substrates for application of BCP to obtain various BCP ordering morphologies of thin films. The distinct characteristics of the two types of the substrate were obtained by different exposure time of UVO treatment (Fig. 1).

Increasing UVO exposure time results in an increase of intensity of the peak (9) that corresponds to –OH stretching in $\equiv$Si–OH (3050–3700 cm^{-1}) (Fig. 2). Similar increase in intensity of the peaks (2) and (3) is expectedly due to oxidation of the –CH_3 group into hydrophilic –OH functional groups at the surface. A hydrophobic to hydrophilic conversion of the functional groups at the surface yields in a decrease of intensity of the peaks (1), (7) and (8) as well, due to a decrease in the amount of the –CH_3 groups at the PDMS surface. The characteristic $\equiv$Si–O–Si$\equiv$ peak (5) decreases when UVO time increases, suggesting that a chain scission occurred in the PDMS system. Similar observations regarding the surface treatment effects on the PDMS surface chemical composition were achieved by exposure to ultraviolet (UV) radiation, UVO treatment, and O_2 plasma treatments of the PDMS substrates, as reported in the literature [50, 51]. Importantly, it is a well-known fact that UVO treatment is far more effective than UV radiation without ozone in creating the hydrophilic –OH groups at the PDMS surface despite the demonstrated effectiveness of the UV radiation treatment on the chain scission at the main polymer backbone [50, 51].

As demonstrated by FTIR, an increase in exposure to the UVO treatment time yields in an enhanced hydrophilicity of the surface of the PDMS substrates. To evaluate this effect, the surface energy of the system corresponded to different exposure times was calculated. Static sessile contact angle measurements for different liquids on UVO-exposed and non-exposed PDMS samples were performed by the Owens-
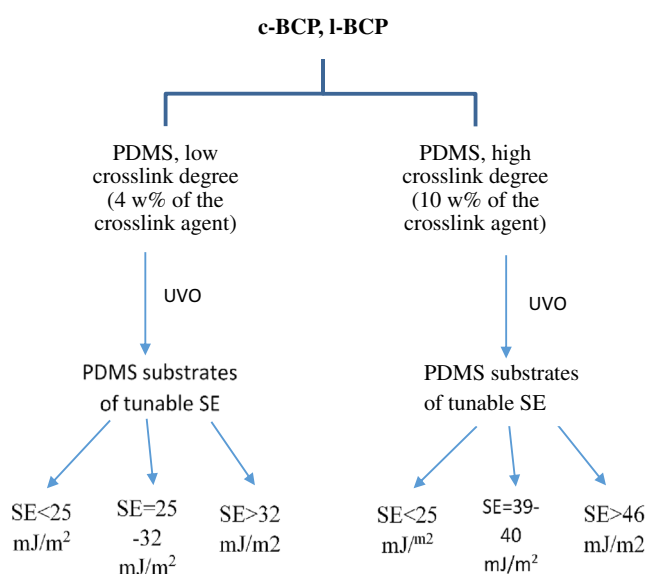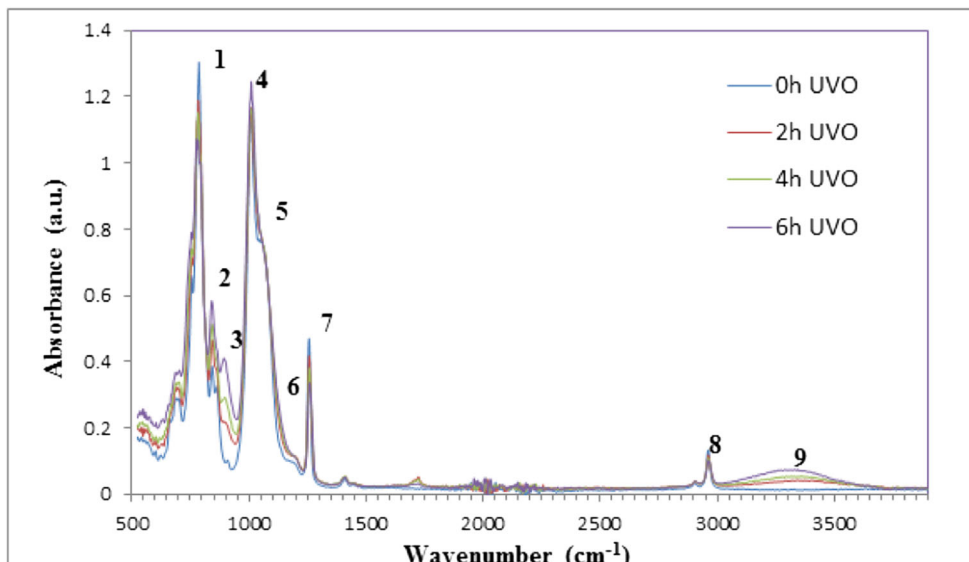

Fig. 1 Schematic demonstration of the experimental conditions used in this study

Fig. 2 FTIR spectra for PDMS films exposed to UVO treatment for various time periods

Wendt method to determine the surface energy [52, 53] by the following equation:

$$\frac{\gamma_L(1 + \cos\theta)}{2\sqrt{\gamma_L^D}} = \frac{\sqrt{\gamma_S^P}\sqrt{\gamma_L^P}}{\sqrt{\gamma_L^D}} + \sqrt{\gamma_S^D} \tag{1}$$

where γ_L and γ_S are the surface free energies for the liquid and the solid interfaces with their saturated vapor, respectively, also here, the superscripts P and D corresponds to the polar and dispersive (non-polar) force components, and $\cos\theta$ is the contact angle [54].

The UVO exposure time versus UVO dose is demonstrated in Fig. 3(a). Increasing surface treatment time is related to an increase of the applied UVO dose and leads to higher surface energy values for PDMS substrates surface. The effect of the UVO dose on the surface energy for both types of the cross-linked PDMS for the compositions containing different amounts of the cross-link agent (4 wt% and 10 wt%) is shown in Fig. 3(b). The UVO lamp to the sample stage distance was set at a constant value of 50 mm.

As shown in Fig. 3(b), SE of PDMS substrates increases from 20 to 62 mJ/m^2 rapidly until UVO exposure dose reaches 100 J/m^2, due to the increasing amount of the hydrophilic –OH groups as demonstrated by increasing intensity at 3050–3600 cm^{-1} (see Fig. 2). Further increase of the dose results in a slow change in the SE until reaching 70 mJ/m^2 (Fig. 3(b)). This large hydrophobic to hydrophilic transition enables us to investigate the dewetting and wetting characteristics of the cast BCP films depending on the cross-link degree/modulus and SE properties of the substrate.

Investigation of the dewetting-wetting behavior of the BCP films is crucial for understanding the conditions of the film stability, which is relevant in most technological applications. The optical micrographs in Fig. 4(a–j) shows the wettability characteristics of the BCP films applied on a PDMS substrate
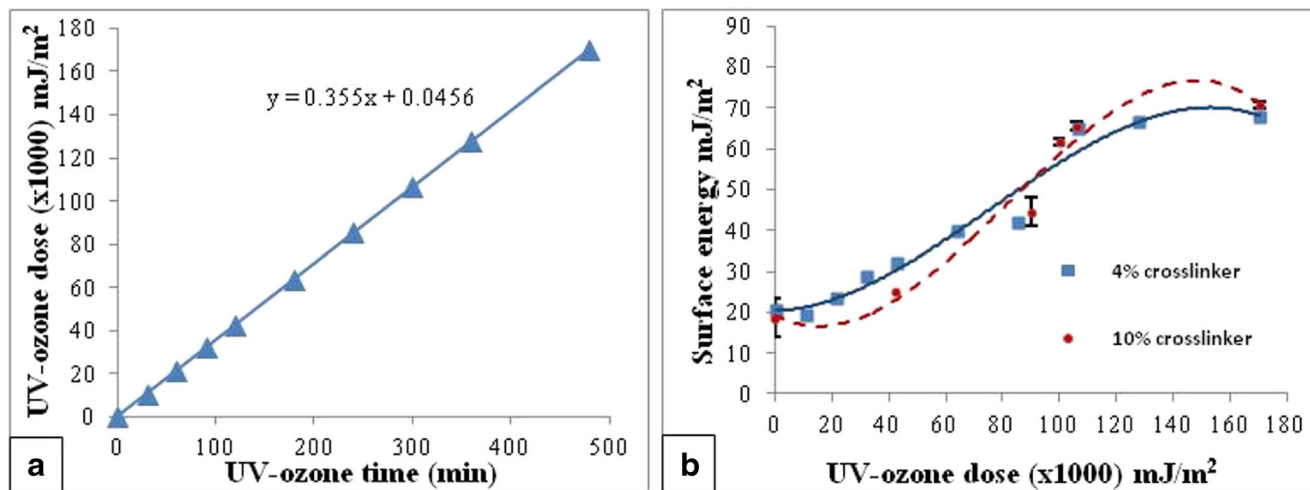

Fig. 3 UVO dose depending on time for the UVO exposure (a) and dependence of the surface energy of PDMS substrates prepared from different compositions on UVO exposure dose (b)

Fig. 4 Optical microscopy images of annealed PS-*b*-PMMA (a–e) for c-BCP (85 nm) and (f–j) l-BCP (75 nm) films on PDMS with increasing SE 20–42 mJ/m². All scale bars are 100 μm

Cylindrical **Lamellar**

Increasing Surface Energy (mJ/m²)

20

24

32

40

42
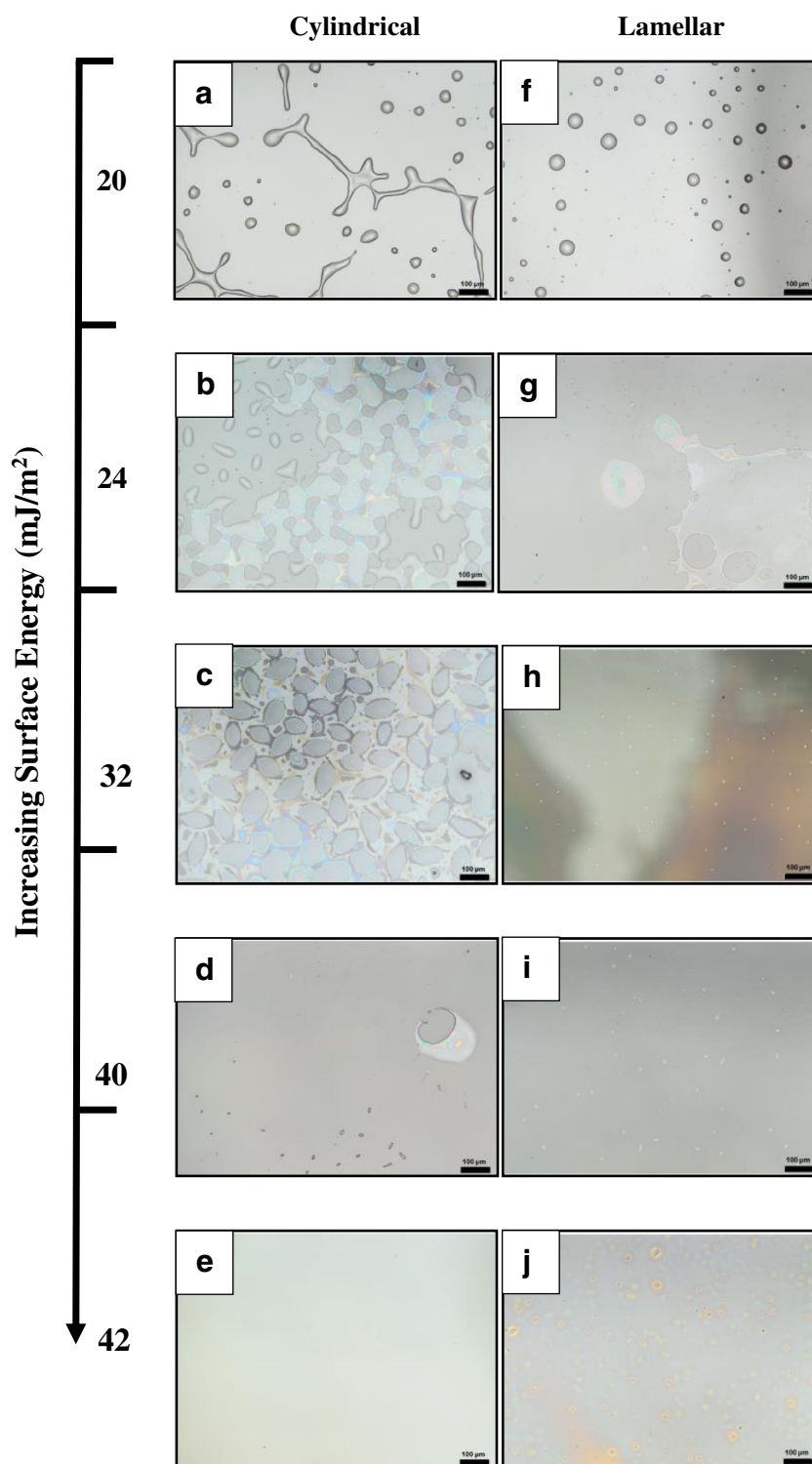
with the lowest cross-link degree (4 wt% of the cross-link agent in the composition) and gradually changing SE after the film annealing. One should note that all the spin-coated BCP films applied on both types of the cross-linked PDMS substrates were initially uniform, regardless of the PDMS cross-link degree and its SE.

The optical micrographs for the annealed c-BCP (Mn 47.5 kg/mol) and l-BCP (Mn 66 kg/mol) of PS-*b*-PMMA films on unexposed to UVO PDMS substrates (4% of the cross-linker) are shown in Fig. 4(a and f), respectively. Non-modified by UVO PDMS substrates (SE~ 20 mJ/m2) have hydrophobic surface characteristics. In this case, the substrate

SE is lower than the sum of the BCP SE and the interfacial tension between substrate and the polymer (S < 0), therefore, it results in film dewetting with various distributions of small, large, and some interconnected BCP droplets on the PDMS surface with decreasing films inhomogeneity corresponded to a diminished dewetting process with increasing SE of the substrate. This is consistent with previously demonstrated late stage dewetting of BCP films due to instability driven breakup of the films after their annealing [33, 35, 54].

At a higher SE (24 mJ/m²) of PDMS, c-BCP films generate important interconnected regions comprising of blend of holes, owing to a transition between early and late stages of dewetting, as shown in Fig. 4(b). Figure 4(g) demonstrates that l-BCP films undergo only hole formation at this early stage of dewetting. Such slow dewetting kinetics can be associated with a larger PMMA fraction of the l-BCP wetting the substrate, compared with c-BCP films. This can additionally be affected by a higher overall MW of the l-BCP compared with the c-BCP. When SE of the PDMS substrates reaches 32 mJ/m², (see Fig. 4(c)), the dewetting trend continues for all the BCP systems, with the lamellar forming BCP films exhibiting more suppressed dewetting behavior than the cylindrical BCP films. We would like to repeat that the annealing conditions of 160 °C for 14 h used during the procedure is quite harsh suggesting that dewetting is intensely retarded at PDMS of SE of 32 mJ/m². On the other hand, l-BCP indicates non-uniform thickness wetting films macroscopically (Fig. 4(h)). The PDMS surface forms a partially to a completely wettable regions due to being in a transition zone. Undoubtedly, further kinetics studies are required to probe the dewetting, inhomogeneous wetting, and uniform BCP film wetting processes, however, this is outside of scope of the present study.

Based on the strong dewetting behavior of c-BCP and l-BCP films applied on non-modified PDMS substrates (SE ~ 20 mJ/m²), we do not anticipate formation of a grafted brush layer similar to the one reported by Limary et al., as the surface chemical composition of PDMS surface with such a low surface energy would presumably prevent grafting [31]. For the PDMS substrates with a higher surface energy, we do not expect presence of a grafted layer since dewetting is progressively stabilized for both cylinder and lamellae forming BCPs, rather than breakup taking place for the entire film. Evidence for a stable wetting regime for both cylinder and lamellar BCP films on the UVO-exposed PDMS substrates with SE above 40 mJ/m² like film breakup or droplet formation is not visible as can be seen in Fig. 4(e and j), respectively. Since both PS and PMMA surface energy values are near to the substrate SE (36–40 mJ/m²) hence, it is an expected result and, therefore, the spreading parameter is expected to be either equal or larger than zero (S ≥ 0). This wetting regime for PS-b-PMMA on PDMS with AFM in examined and depicted in detail (Fig. 5).
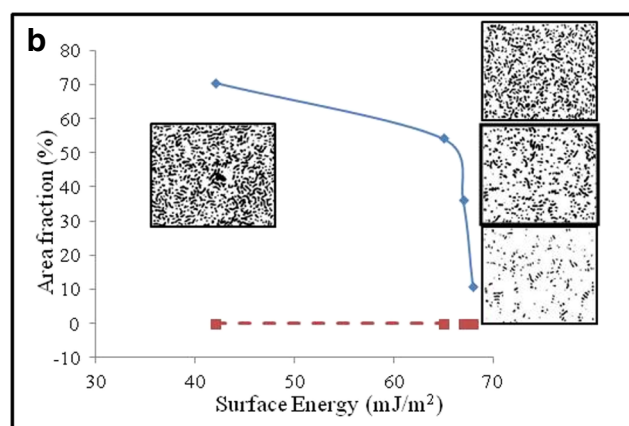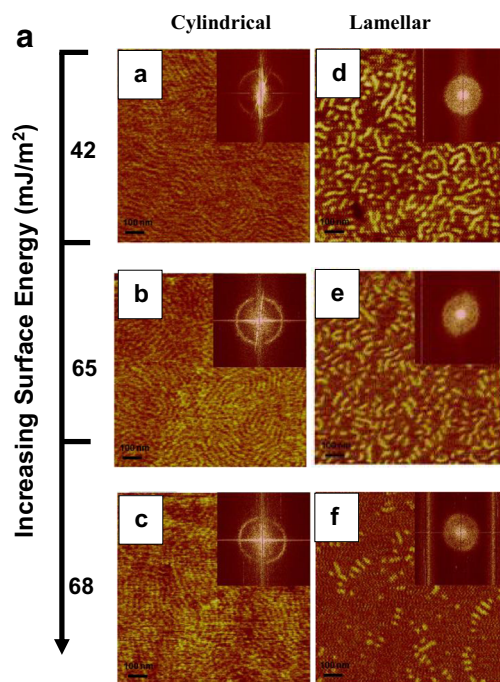

Fig. 5 (A) AFM phase images. (a–c) c-BCP (PS-b-PMMA, M_w 35-b-12.5 kg/mol) on PDMS substrates (lowest cross-link degree, 4 wt% of the cross-linking agent, SE = 42, 65, 68 mJ/m²), (d–f) l-BCP PS-b-PMMA (M_w 33-b-33 kg/mol) on PDMS substrates (lowest cross-link degree, 4 wt% of the cross-linking agent, SE = 42, 65, 68 mJ/m². All the scale bars are of 100 nm. (B) The area fraction (%) of the perpendicular orientated lamellar (solid line) and cylindrical (dashed line) for PS-b-PMMA films on PDMS substrates (lowest cross-link degree, 4 wt% of the cross-link agent)

The BCP morphologies of c-BCP and l-BCP (PS-b-PMMA) films on PDMS substrates with the lowest cross-link degree (4% of the cross-linker in the composition) investigated using AFM are illustrated in Fig. 5(A (a–c) and (d–f)), respectively (see Section 2 for detailed sample preparation). As one would expect, the cylindrical PS-b-PMMA demonstrate almost 100% parallel orientation on PDMS substrate with SE of 42 mJ/m². This is what one would anticipate, since the PMMA cylinder block is of a higher polarity compared to the PS block, and it is typically more attracted to the oxidized

surface, such as the UVO modified PDMS, forming parallel cylinders. The fully parallel orientation remains stable with an increased dose of the UVO treatment that corresponds to SE of 42–70 mJ/m^2. This is consistent with the FFT of the AFM images shown in the upper insets of the Fig. 5(A a–c).

The lamellae forming PS-*b*-PMMA films indicate a transition from typically perpendicular to gradually increasing mixed morphology, since the substrate surface energy is changed from 42 to 68 mJ/m^2 (Fig. 5(A e–h)). Figure 4B shows the fraction of the morphology with perpendicular oriented both c-BCP and l-BCP films. Unlike the cylinder fraction, which does not change within the entire SE range of 42–70 mJ/m^2, the perpendicular orientated lamellar in BCP films gradually transform to parallel orientated for the BCP films applied on the PDMS substrates with the surface energy of 65 mJ/m^2 (23% change) and change almost completely around 70 mJ/m^2 (85% change). To our knowledge, the difference in BCP morphology between the cylindrical and the lamellae forming BCP applied on the substrates with different cross-link degree/flexibility has not been previously investigated. Our gradually altered SE of the substrates allowed for obtaining a range of surface characteristics to make this comparative study.

Agreeing with the theoretical simulations and predictions of Sommer et al. [55, 56], an equilibrium of the stretching energy of diblock copolymers at the surface of the film with the substrate favors the lamellae forming BCP rather than the cylindrical ones. As demonstrated by these simulations, the increase in the BCP radius of gyration, Rg, with the segregation strength, χN, is stronger for the symmetric BCP that maintain a perpendicular orientation on the substrates with the neutral surface energy. This is in agreement with our previous observations which determined that the perpendicular morphology of the lamellae forming BCP is steady over an extended surface energy range, compared to the cylinder forming BCP.

We performed related experiments in order to determine whether the substrate flexibility plays a role in this transition, on the PDMS substrates with a higher cross-link degree (10 wt% of the cross-linker) and higher modulus. The dewetting and wetting characteristics, as well as the morphology changes for the cylinder forming PS-

b-PMMA films applied on the UVO-exposed PDMS substrates (10 wt% of the cross-linker) follow from the optical micrographs and AFM images in Fig. 5 (a–c) and (d–f), respectively.

When the substrate SE is close to that of the non-modified PDMS (22 mJ/m^2), the c-BCP films displays holes formation, which is proof of an early stage of dewetting of the polymer films. It seems that small variations (e.g., 20 mJ/m^2 versus 22 mJ/m^2) in the SE may occur with changes of the cross-link degree. These changes, for instance, between 20 and 24 mJ/m^2 can significantly influence the rate of the dewetting

as it was discussed above and demonstrated in Fig. 4. Thus, it is difficult to conclude if the slow rate of the hole formation on a non-modified 10% PDMS versus the fast rate of the dewetting on a non-modified lower cross-link density PDMS is due to SE variation or modulus alteration. Numerous studies have been carried on how the viscoelasticity of the substrate affects dewetting of polymers in a bilayer form [57].

Intuitively, the BCP film wetting characteristics are anticipated to be upgraded with an upsurge in the SE at the top surface of PDMS. A partially suppressed dewetting part of the film was observed, where the dewetting to wetting transition can be comprehended with a small change in the PDMS SE shown in Fig. 6(b) (27 mJ/m^2). Yet, a stable continuous film on an elastomeric substrate was not visible at this stage. Further treatment of the PDMS substrate with UVO leads to enhancement of the wettability of the BCP films at a higher SE of 38 mJ/m^2, which is close to that of the SE of each block.

The c-BCP morphology is illustrated in AFM images in Fig. 6(d–f) from dewetting to wetting transition. The AFM images shown in the optical micrographs in Fig. 5(b) for the PS-*b*-PMMA films applied on a PDMS substrate with the SE of 27 mJ/m^2 in the wetting region revealed mostly perpendicular orientation of the PMMA cylinders. As far as the vertical orientation is considered, the coherent wetting sections of the films are dependent on the point that the c-BCP blocks are based on a repulsive yet close to neutral SE substrates. Alternatively, the dewetting may possibly have induced vertical alignment based on the parameters of the process of dewetting hole formation. Nevertheless, we observed that there is an absence of the long-range order of the perpendicular cylinders all over these wetting regions of the film.

Further, increase in the SE from 38 to 70 mJ/m^2 due to a higher amount of the hydrophilic functional groups on the surface yields in a complete wetting of the PDMS substrates by the BCP films as shown in Fig. 5(e, f). Presumably, wetting of the PMMA block is enhanced with an increasing of the SE of PDMS substrates in the SE range of 38–70 mJ/m^2, resulting in a parallel orientation of the PMMA cylinders within the PS matrix of the BCP films on the PDMS.

Grazing-incidence small-angle X-ray scattering (GISAXS) experiments were done for these c-BCP PS-PMMA thin films to probe their morphology, as shown in lower insets of Fig. 5(e, f). The GISAXS images show a mixed overall film morphology (i.e., horizontal and vertical cylinders) adjacent to the transition zone (38 mJ/m^2), in the cases where only parallel cylinder orientation controls the film-air interface (Fig. 6(e)). Evidently, this fraction of the vertically oriented cylinders must be located in the interior part of the film, and possibly, even near the interface with the close-to-neutral surface energy PDMS substrate as well. For the substrate SE of 68 mJ/m^2, the GISAXS spectra for c-BCP film on such highly hydrophilic surface show intense scattering peaks indicating a

Fig. 6 BCP film wettability and the morphology varying with the c-BCP PS-*b*-PMMA (M_w 35–12.5 kg/mol) films on PDMS substrates annealed at 160 °C; Optical images for BCP films on PDMS substrates with the substrate SE of (a) 22 mJ/m², (b) 27 mJ/m², and (c) 38 mJ/m² and AFM phase images for the BCP films on PDMS substrates with the substrate SE of (d) 27 mJ/m², (e) 38 mJ/m², and (f) 68 mJ/m². Scale bars for OM and AFM images are 100 μm and 100 nm, respectively
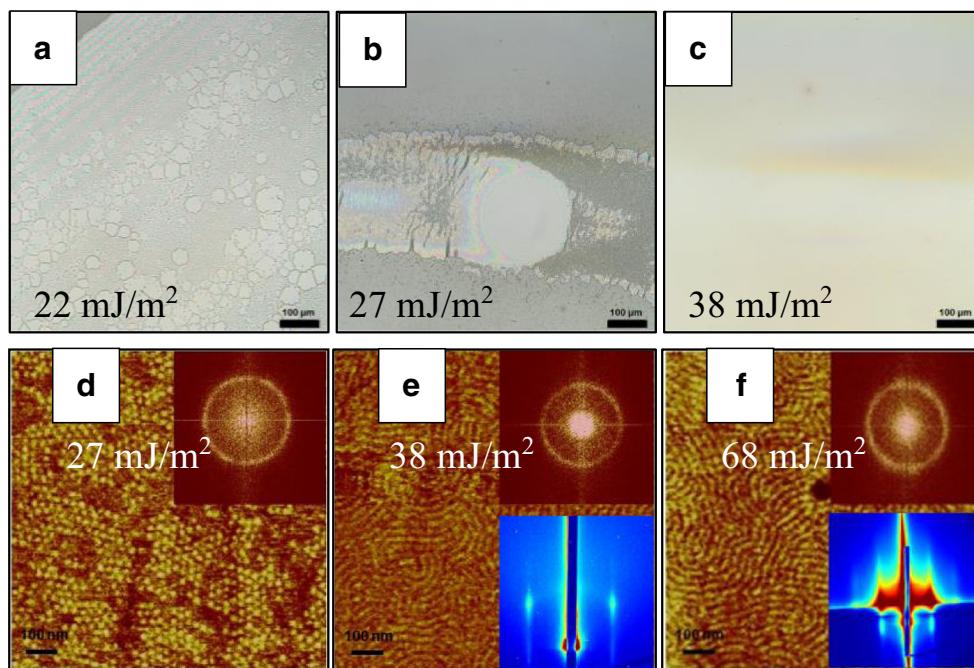
significant increase in the parallel oriented cylinder fraction (Fig. 6(f) versus (e) inset GISAX scattering pattern) all over the film, (i.e., at the surface and in bulk), steady with the overall film morphology arising from a higher degree of the substrate wetting via the parallel oriented PMMA cylinders.

In case of the l-BCP films on the UVO-treated PDMS substrates with a higher cross-link degree (10 wt% of the cross-linking agent), the optical micrographs are shown in Fig. 6(a–d) and AFM the images are illustrated as insets of the Fig. 6. In contrast to the early stage dewetting of c-BCP films on hydrophobic PDMS substrates with the SE = 22 mJ/m², the l-BCP films do not follow similar dewetting trend in the same SE range, as shown in Fig. 6(a). We observe a film cracking rather than dewetting on the non-modified l-BCP films with a higher cross-link degree (10 wt% of the cross-linking agent), which is typically related to adhesion issues. A higher modulus of the substrate with a higher cross-link degree and a slightly higher SE and a higher molecular weight of the BCP may all contribute to these cracking phenomena that will be further studied in detail and reported separately.

We obtained uniform films for PDMS with SE above 27 mJ/m², as reported in Fig. 6 (b–d). AFM images for the l-BCP films on PDMS substrates with a wide SE range of 22–68 mJ/m² are shown in Fig. 6(a–d) as insets. It is noteworthy that clear AFM images are tough to get in some cases for the BCP films because of a low compliance of the underlying PDMS substrates. In contrast to the c-BCP surface, the lamellar forming BCP regions generally align perpendicularly on 10% cross-linked PDMS substrates at almost all the SE range (22–68 mJ/m²). Comparing the continuity of the perpendicular lamellae domains in the BCP films on the PDMS with the lower cross-link degree (4 wt% of the cross-linker), larger areas of perpendicularly aligned lamellae domains are observed on the substrates with a higher cross-link degree (10 wt% of the cross-linker). To establish the uniform morphology throughout the films, the GISAXS measurements were done on the lamellar forming PS-PMMA thin films cast on PDMS substrates, as displayed in the lower insets of Fig. 6(b–d). The GISAXS results are consistent with the transition of the lamellar structure from the vertically oriented (Fig. 6(b)) to horizontally oriented (Fig. 7(d)). This is qualitatively similar to what is observed for the morphology of the films applied on the PDMS with the lower cross-link degree (4 wt% of the cross-linker) and increasing SE. Quantitative differences in the orientation behavior of the BCP films may be related to the flexibility of the PDMS substrate.

Additionally, as it is well known, PDMS is known for being able to recover partially its SE upon plasma modification [58], a result attributed to the presence of non-cross-linked monomers at the surface. To determine whether the potential substrate surface energy recovery via the non-cross-linked monomers has affected our BCP orientation in any way or not, we performed a qualitative research of a solvent extraction with three different solvents and over several days to remove the on-cross-linked monomers from the PDMS network prior to the UVO treatment, followed by the BCP annealing. The morphology of these BCP films depicted the non-extracted films orientation on the PDMS substrates within permissible experimental error. We conclude that the surface restructuring of the non-cross-linked fraction of the PDMS monomers do not affect our BCP orientation study in any way whatsoever, and possibly does not happen in BCP coated PDMS substrates.
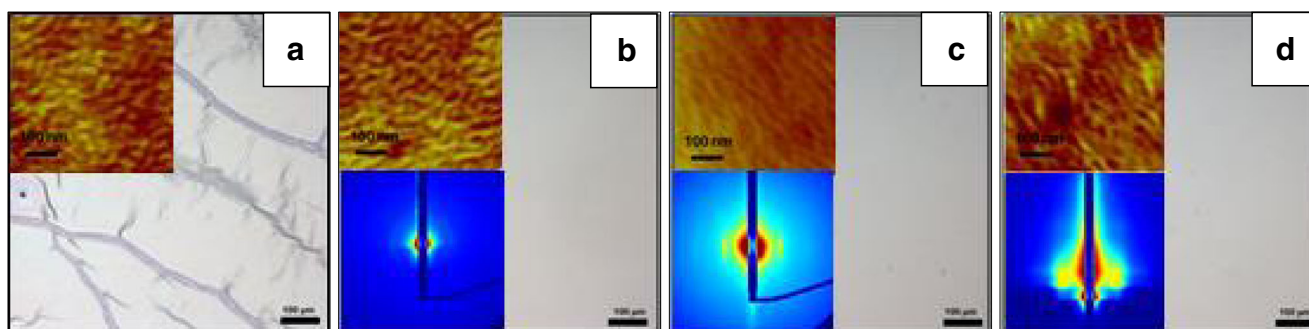
Fig. 7 BCP film wettability and morphological variation for the l-BCP films (M_w 33–33 kg/mol) on PDMS substrates annealed at 160 °C; Optical and AFM (inset left top corner) images for the BCP films on the PDMS substrates with the substrate SE = (a) 22 mJ/m^2, (b) 27 mJ/ m^2, (c) 38 mJ/m^2, (d) 68 mJ/m^2; GISAXS images (inset) for the BCP films on the PDMS substrates with the SE of (b) 27 mJ/m^2, (c) 38 mJ/m^2, (d) 68 mJ/m^2. Scale bars for OM and AFM images are 100 μm and 100 nm respectively

A final comment is that PDMS will exert a compressive stress upon cooling below the Tg of the BCP film, due to its coefficient of thermal expansion, $\alpha \sim 325 \cdot 10^{-6}$ °C, which is five times higher than that of the PS-*b*-PMMA film ($\alpha_{PS} = 60 \cdot 10^{-6}$-$80 \cdot 10^{-6}$ °C, $\alpha_{PMMA} = 50 \cdot 10^{-6}$ °C) [59]. As far as buckling is considered for the composite bilayer upon cooling, the compression is quite small at cooling from the BCP Tg (100 °C), to the ambient 25 °C, hence no practical buckling is observed, although partial cracking can be present in exceptional cases (Fig. 7a). For the PDMS with a lower cross-link degree (4 wt% of the cross-linker), it is expected to be proportionally lower and the compression is also insufficient to buckle the BCP film.

4 Conclusions

Motivated by needs for flexible electronics of the future, particularity related to directed self-assembly (DSA) of BCPs on flexible substrates, we have mapped a large range of two BCP morphologies and studied their surface phenomena from dewetting to partial wetting to complete wetting on modified SE and varied flexibility/modulus PDMS substrates. The substrate SE variation from hydrophobic to hydrophilic was organized by using the UVO treatment. In the wetting regime, we inspected the molecular orientation behavior of the c-BCP and l-BCP films on elastomeric PDMS substrates. Specifically, a strong dewetting was observed for both c-BCP and l-BCP on PDMS substrates with SE below 25 mJ/m^2 and the lowest cross-link degree. The dewetting behavior is more retarded for the l-BCP (higher Mw) compared with the c-BCP (lower Mw). Whether the dewetting kinetics is affected more by Mw or by the morphology will be a scope of a future study.

This is followed by a regime of partial dewetting for both c-BCP and l-BCP with SE above 25 mJ/m^2 and below 32 mJ/m^2 on the same cross-linked PDMS substrates (4 wt% of the cross-linker). The transition from dewetting to wetting regions is rapid for the l-BCP than for the c-BCP films at this stage. A complete wetting was witnessed for both l-BCP and c-BCP PS-*b*-PMMA films, at the conditions where the substrate SE is above 32 mJ/m^2 (and 25 mJ/m^2) for both types of the cross-linked PDMS substrates. Evidently, a higher SE is required for both l-BCP and c-BCP film to undergo wetting on the more flexible PDMS substrates.

For PDMS with SE above 40 mJ/m^2, potentially because of the higher intrinsic stability of the l-BCP, its outer surface remains perpendicular and decays very slowly with increasing SE up to 70 mJ/m^2. This is important and relevant to applications of such vertically oriented lamellae. In contrast, perpendicular cylinders are observed only for the films applied on PDMS with a narrow SE window around 40 mJ/m^2, with mostly parallel orientation on the substrates with SE above 40 mJ/m^2. These results can have widespread practical usage for flexible substrates based on BCP nanoelectronics technology, such as next-generation organic solar cells that need flexible substrates.

References

1. R.A. Segalman, Patterning with block copolymer thin films. Mater. Sci. Eng. R Rep **48**, 191–226 (2005)

2. S.H. Kim, M.J. Misner, T. Xu, M. Kimura, T.P. Russell, Highly Oriented and Ordered Arrays from Block Copolymers via Solvent Evaporation. Adv. Mater. **16**, 226–231 (2004)

3. S.B. Darling, P. Polym, Sci. **32**, 1152–1204 (2007)

4. S. Park, D.H. Lee, J. Xu, B. Kim, S.W. Hong, U. Jeong, T. Xu, T.P. Russell, Macroscopic 10-Terabit–per–Square–Inch Arrays from

Block Copolymers with Lateral Order. Science **323**, 1030–1033 (2009)

5. Y.A. Elabd, M.A. Hickner, Block Copolymers for Fuel Cells. Macromolecules **44**, 1–11 (2011)

6. R.A. Segalman, B. McCulloch, S. Kirmayer, J.J. Urban, Block Copolymers for Organic Optoelectronics. Macromolecules **42**, 9205–9206 (2009)

7. C.T. Black, K.W. Guarini, K.R. Milkove, S.M. Baker, T.P. Russell, M.T. Tuominen, Integration of self-assembled diblock copolymers for semiconductor capacitor fabrication. Appl. Phys. Lett. **79**, 409–411 (2001)

8. E.W. Edwards, M.P. Stoykovich, H.H. Solak, P.F. Nealey, Long-range order and orientation of cylinder-forming block copolymers on chemically nanopatterned striped surfaces. Macromolecules **39**, 3598–3607 (2006)

9. X.M. Yang, R.D. Peters, P.F. Nealey, Source **33**, 9575–9582 (2000)

10. T. Xu, Y. Zhu, S.P. Gido, t.P. Russell, Electric Field Alignment of Symmetric Diblock Copolymer Thin Films. Macromolecules **37**, 2625–2529 (2004)

11. M.W. Matsen, Electric Field Alignment in Thin Films of Cylinder-Forming Diblock Copolymer. Macromolecules **39**, 5512–5520 (2006)

12. M. Park, Block Copolymer Lithography: Periodic Arrays of 1011 Holes in 1 Square Centimeter. Science **276**, 1401–1404 (1997)

13. R. Ruiz, H. Kang, F.A. Detcheverry, E. Dobisz, D.S. Kercher, T.R. Albrecht, J.J. de Pablo, P.F. Nealey, Density Multiplication and Improved Lithography by Directed Block Copolymer Assembly. Science **321**, 936–939 (2008)

14. G. Singh, K.G. Yager, D.N. Smilgies, M.M. Kulkarni, D. Bucknall, A. Karim, Tuning Molecular Relaxation for Vertical Orientation in Cylindrical Block Copolymer Films via Sharp Dynamic Zone Annealing. Macromolecules **45**(17), 7107–7117 (2012)

15. P. Samaddara, A. Deepb, K.-H. Kim, An engineering insight into block copolymer self-assembly: Contemporary application from biomedical research to nanotechnology. Chem. Eng. J. **342**, 71–89 (2018)

16. N. Mahadevapuram, I. Mitra, S. Sridhar, S. Strzalka, G.E. Stein, Ordering of lamellar block copolymers on oxidized silane coatings. Eur. Polym. J. **75**, 495–503 (2016)

17. R. Raharjo, B. Freeman, D. Paul, G. Sarti, E. Sanders, Pure and mixed gas CH4 and n-C4H10 permeability and diffusivity in poly(-dimethylsiloxane). J. Memb. Sci. **306**, 75–92 (2007)

18. F. Abbasi, H. Mirzadeh, A.A. Katbab, Modification of polysiloxane polymers for biomedical applications: a review. Polym. Int. **50**, 1279–1287 (2001)

19. N. Fong, A. Simmons, L. Poole-Warren, Elastomeric Nanocomposites **9**, 257–280 (2011)

20. D. Wang, D. Ba, Z. Hao, F. Y Li, K. Sun, G. Du Liu, Q. Mei, A novel approach for PDMS thin films production towards application as substrate for flexible biosensors. Mater. Letters. **221**, 228–231 (2018)

21. Y.-C. Yeh, E.A. Corbin, S.R. Caliari, R. Ouyang, S.L. Vega, R. Truitt, L. Han, K.B. Margulius, J.A. Burdick, Biomater **145**, 23–32 (2017)

22. D.Y. Khang, J.A. Rogers, H.H. Lee, Adv. Funct. Mater. **19**, 1526–1536 (2008)

23. J.A. Rogers, T. Someya, ; Huang, Y. Materials and mechanics for stretchable electronics. Science (80-.). 2010, **327**, 1603–1607

24. J. Liu, Z. Wang, P. Zeng, M. Song, W. Huang, Z. Liu, Z. Xu, J. Li, C. Liu, Y. Jiang, Direct casting of a PDMS substrate holder from a structured polymer film for lab-on-a-foil bonding. Sensors Actuators B **266**, 570–576 (2018)

25. Y. Sun, W.M. Choi, H. Jiang, Y.Y. Huang, J.A. Rogers, Controlled buckling of semiconductor nanoribbons for stretchable electronics. Nat. Nanotechnol. **1**, 201–207 (2006)

26. H. Jiang, Y. Sun, J.A. Rogers, Y. Huang, Mechanics of precisely controlled thin film buckling on elastomeric substrate. Appl. Phys. Lett. **90**, 133119 (2007)

27. S. Park, D.H. Lee, T.P. Russell, Self-Assembly of Block Copolymers on Flexible Substrates. Adv. Mater. **22**, 1882–1884 (2010)

28. G. Singh, K.G. Yager, B. Berry, H.C. Kim, A. Karim, ACS Nano (2012)

29. O.K.C. Tsui, T.P. Russell, *Polymer Thin Film* (World Scientific Publishing Co.Pte. Ltd., Singapore, 2008)

30. R. Limary, P.F. Green, Dewetting Instabilities in Thin Block Copolymer Films: Nucleation and Growth. Langmuir **15**, 5617–5622 (1999)

31. J.W. Cahn, Phase Separation by Spinodal Decomposition in Isotropic Systems. J. Chem. Phys. **42**, 93–99 (1965)

32. B. Wei, J. Genzer, R.J. Spontak, Dewetting Behavior of a Block Copolymer/Homopolymer Thin Film on an Immiscible Homopolymer Substrate. Langmuir **20**, 8659–8667 (2004)

33. G. Reiter, Unstable thin polymer films: rupture and dewetting processes. Langmuir **9**, 1344–1351 (1993)

34. G. Reiter, Dewetting of thin polymer films. Phys. Rev. Lett. **68**, 75–78 (1992)

35. R. Limary, P.F. Green, K.R. Shull, Influence of surface ordering on the wetting of structured liquids. Eur. Phys. J. E. Soft Matter **8**, 103–110 (2002)

36. J.L. Masson, R. Limary, P.F. Green, Pattern formation and evolution in diblock copolymer thin films above the order–disorder transition. J. Chem. Phys. **114**, 10963 (2001)

37. R.D. Peters, X.M. Yang, T.K. Kim, P.F. Nealey, Wetting Behavior of Block Copolymers on Self-Assembled Films of Alkylchlorosilanes: Effect of Grafting Density. Langmuir **16**, 9620–9626 (2000)

38. C. Huang, G. Wen, J. Li, T. Wu, L. Wang, T. Wu, L. Wang, F. Xue, H. Li, T. Shi, J. Coll, Interface Sci. **478**, 236–245 (2018)

39. P. Mansky, T. Russell, C. Hawker, J. Mays, D. Cook, S. Satija, Phys. Rev. Lett. **29**, 237–240 (1997)

40. P. Mansky, Y. Liu, E. Huang, T.P. Russell, C. Hawker **275**, 1458–1460 (1997)

41. G.J. Kellogg, D.G. Walton, A.M. Mayes, P. Lambooy, T.P. Russell, P.D. Gallagher, S.K. Satija, Observed Surface Energy Effects in Confined Diblock Copolymers. Phys. Rev. Lett. **76**, 2503–2506 (1996)

42. E. Huang, T.P. Russell, C. Harrison, P.M. Chaikin, Using Surface Active Random Copolymers To Control the Domain Orientation in Diblock Copolymer Thin Films. Macromolecules **31**, 7641–7650 (1998)

43. E. Huang, S. Pruzinsky, T.P. Russell, J. Mays, C.J. Hawker, Neutrality Conditions for Block Copolymer Systems on Random Copolymer Brush Surfaces. Macromolecules **32**, 5299–5303 (1999)

44. D.Y. Ryu, K. Shin, E. Drockenmuller, C.J. Hawker, T.P. Russell, A Generalized Approach to the Modification of Solid Surfaces. Science **308**, 236–239 (2005)

45. D.Y. Ryu, S. Ham, E. Kim, U. Jeong, C.J. Hawker, T.P. Russell, Cylindrical Microdomain Orientation of PS-b-PMMA on the Balanced Interfacial Interactions: Composition Effect of Block Copolymers. Macromolecules **42**, 4902–4906 (2009)

46. S.O. Kim, H.H. Solak, M.P. Stoykovich, N.J. Ferrier, J.J. De Pablo, P.F. Nealey, Epitaxial self-assembly of block copolymers on lithographically defined nanopatterned substrates. Nature **424**, 411–414 (2003)

47. J. Heier, J. Genzer, E.J. Kramer, F.S. Bates, S. Walheim, G. Krausch, Transfer of a chemical substrate pattern into an island-forming diblock copolymer film. J. Chem. Phys. **111**, 11101 (1999)

48. A.P. Smith, A. Sehgal, J.F. Douglas, A. Karim, E.J. Amis, Combinatorial Mapping of Surface Energy Effects on Diblock

Copolymer Thin Film Ordering. Macromol. Rapid Commun. **24**, 131–135 (2003)

49. Z. Wang, A.A. Volinsky, N.D. Gallant, Crosslinking effect on poly-dimethylsiloxane elastic modulus measured by custom-built compression instrument. J. Appl. Polym. Sci. **131** (2014). https://doi.org/10.1002/APP.41050

50. K. Efimenko, Surface Modification of Sylgard-184 Poly(dimethyl siloxane) Networks by Ultraviolet and Ultraviolet/Ozone Treatment. J. Colloid Interface Sci. **254**, 306–315 (2002)

51. C. De Menezes Atayde, I. Doi, C.D.M. Atayde, Phys. Status Solidi **7**, 189–192 (2010)

52. S. Wu, *Polymer Interface and Adhesion* (Marcel Dekker, New York, 1982)

53. K.L. Mittal, *Contact Angle, Wettability and Adhesion* (VSP, Utrecht, 1993)

54. D.K. Owens, R.C. Wendt, Estimation of the surface free energy of polymers. J. Appl. Polym. Sci. **13**, 1741–1747 (1969)

55. A. Hoffmann, J.U. Sommer, A. Blumen, Computer simulations of asymmetric block copolymers. J. Chem. Phys. **107**, 7559–7570 (1997)

56. J.U. Sommer, A. Hoffmann, A. Blumen, Block copolymer films between neutral walls: A Monte Carlo study. J. Chem. Phys. **111**, 3728–3732 (1999)

57. A. Faldi, R.J. Composto, K.I. Winey, *Unstable polymer bilayers. 1. Morphology of Dewetting* (1996), pp. 4855–4861

58. J.N. Lee, C. Park, C.; G.M. Whitesides, Anal. Chem. 2003, 75, 6544–6554, Solvent Compatibility of Poly(dimethylsiloxane)-Based Microfluidic Devices

59. J.E. Mark, *Polymer Data Handbook* (Oxford University Press, Inc, New York, 1999)